Pu Zhaoxia (Orcid ID: 0000-0003-4461-1789)
Tallapragada Vijay (Orcid ID: 0000-0003-4255-897X)
Atlas Robert (Orcid ID: 0000-0002-0706-3560)
Ruf Christopher, S (Orcid ID: 0000-0002-5937-4483)

A Preliminary Impact Study of CYGNSS Ocean Surface Wind Speeds on Numerical Simulations of Hurricanes Harvey and Irma (2017)

Zhiqiang Cui *and* Zhaoxia Pu

Department of Atmospheric Sciences, University of Utah, Salt Lake City, UT

Vijay Tallapragada

Environmental Modeling Center, National Centers for Environmental Prediction, NWS/NOAA, College Park, MD

Robert Atlas

NOAA/Atlantic Oceanographic and Meteorological Laboratory, Miami, FL

Christopher S. Ruf

Department of Climate and Space, University of Michigan, Ann Arbor, MI

Submitted to *Geophysical Research Letters*

February 17, 2019

Key points: The NASA Cyclone Global Navigation Satellite System (CYGNSS) provides an unprecedented opportunity to obtain ocean surface wind data over a hurricane inner-core region. This study found that the assimilation of CYGNSS data results in improved track, intensity, and

structure forecasts for two notable landfalling hurricanes, Harvey and Irma (2017).

Corresponding Author: Prof. Zhaoxia Pu, Department of Atmospheric Sciences, University of Utah, 135 S 1460 E, Rm. 819, Salt Lake City, UT 84112, USA. Email: Zhaoxia.Pu@utah.edu

Abstract

The NASA Cyclone Global Navigation Satellite System (CYGNSS) was launched in December 2016, providing an unprecedented opportunity to obtain ocean surface wind speeds (OSWS) including wind estimates over the hurricane inner-core region. This study demonstrates the influence of assimilating an early version of CYGNSS observations of OSWS on numerical simulations of two notable landfalling hurricanes, Harvey and Irma (2017). A research version of the NCEP operational Hurricane Weather Research and Forecasting model and the Grid-point Statistical Interpolation based hybrid ensemble-3-dimensional variational data assimilation system are used. It is found that the assimilation of CYGNSS data results in improved track, intensity, and structure forecasts for both hurricane cases, especially for the weak phase of a hurricane, implying potential benefits of using such data for future research and operational applications.

1. Introduction

Modern high-resolution numerical models for hurricane prediction that include a suite of sophisticated physical parameterizations have paved the way for obtaining improved tropical cyclone (TC) forecasts in the past few decades, but model deficiencies in physical parameterizations and uncertainties in initial conditions still have a large impact on forecast accuracy (e.g., Gall et al., 2013; Atlas et al., 2015; Otkin et al., 2017). It has been recognized that the lack of frequent and accurate observations of winds in the inner core of TCs (Rogers et al., 2006; 2013) contributes significantly to inaccurate prediction. Previous studies have proved that assimilation of hurricane inner-core observations, such as those from airborne Doppler radar, can result in significant improvements in TC track and intensity forecasts (e.g., Pu et al., 2009; Zhang et al., 2011; Gall et al., 2013; Pu et al., 2016). However, airborne Doppler radar missions are limited in space and time, and many satellites are unable to penetrate the heavy rainfall in a hurricane inner-core region. A recent NASA satellite mission, the Cyclone Global Navigation Satellite System (CYGNSS, Ruf et al., 2016), was launched on December 15, 2016, and was specifically designed to overcome observational deficiencies, as it provides an unprecedented opportunity to obtain ocean surface wind data within a hurricane's inner-core.

CYGNSS is a constellation of eight microsatellites that receive direct Global Positioning System (GPS) signals and scattered signals from the ocean surface. These microsatellites provide detailed ocean surface wind speeds (OSWS) in the tropics. Compared with most space-based measurements that use backscattered microwave radar pulses (e.g. QuikSCAT, ASCAT), GPS

signals are in an L-band frequency and are largely unaffected by precipitation. Therefore, CYGNSS-derived OSWS are available in a TC inner-core region and provide high temporal resolution and spatial coverage under all precipitating conditions and over the full dynamic range of wind speeds experienced in a TC (Ruf et al., 2016; Morris and Ruf, 2017). Before its launch, a variety of observing system simulation experiments (e.g., Annane et al., 2018; Leidner et al., 2018; McNoldy et al., 2017; Zhang et al., 2017) suggested that assimilation of CYGNSS OSWS would have positive impacts on short-range hurricane forecasts of both track and intensity with the Hurricane Weather Research and Forecasting (HWRF) model.

CYGNSS data became available in March 2017. The goal of this study is to demonstrate the impact of a preliminary version of CYGNSS-retrieved OSWS on numerical simulations of hurricanes. Two notable hurricane cases, Harvey and Irma (2017), are used. Considering the significant losses caused by both hurricanes after their landfall, the data impact study emphasizes the period before and near their landfall. The NCEP HWRF model and the Grid-point Statistical Interpolation (GSI) based hybrid ensemble-3-dimensional variational data assimilation system (e.g., 3DEnVar; Wang et al., 2013) are employed to facilitate the data assimilation experiments.

2. CYGNSS data, HWRF model, and experimental design

2.1 CYGNSS data

With the CYGNSS science team's efforts to develop the calibration and retrieval algorithm, the first science-quality CYGNSS on-orbit OSWS data product is Version 2.0 Level 2 retrieved wind speeds, which consist of time-tagged and geolocated average wind speed and

corresponding uncertainty with about a 25 km resolution (Ruf et al., 2018). Considering the quality of retrieved OSWS and the current ability of the HWRF system to assimilate inner-core observations (Zhang et al., 2018), this study uses only the fully developed seas (FDS) version. An alternative, the young seas/limited fetch (YSLF) version of OSWS data is not used here. The YSLF should be better estimates under TC conditions, but the quality of the Version 2.0 YSLF OSWS data is poor and inconsistent with that of the FDS. Figure 1a shows the sample FDS data coverage in four consecutive periods (00UTC, 06UTC, 12UTC, and 18UTC) on 6 September 2017. High-density data cover the Atlantic Ocean and vicinity in at least two periods (e.g., 00UTC and 06UTC). Along each data line, there is no distinct data gap. Even though there are some occasional drop outs near the storm center, these data still reliably represent low to moderate winds (Ruf and Balasubramaniam, 2018).

To obtain the characteristics of the CYGNSS-retrieved OSWS and their associated errors, we take data samples over an area of interest (the domain enclosed by the dashed line in Figure 1a) from 00 UTC 15 August to 00 UTC 16 September 2017, which covers the entire life cycle of both Harvey and Irma, for a statistical analysis. Figure 1b shows that low wind speeds are dominant, while high wind speed are present in smaller quantities out to about 36 m s^{-1}. Figure 1c shows there is a strong dependence of these assigned wind speed errors on wind speed. Most wind observation standard deviations are concentrated below 6 m s^{-1}, and only a small proportion of high wind-speed data corresponds to the high-speed error value (around 10 m s^{-1}). Figure 1b and c also show that the characteristics of CYGNSS data for Hurricanes Harvey and Irma (2017) are consistent with the sample data at large.

2.2 HWRF model and assimilation method

A research version of the NCEP operational HWRF model used is Version 3.9a (Biswas et al., 2017), released by the UCAR Developmental Testbed Center (https://dtcenter.org). The model is configured in a three-level nested domain, with horizontal resolutions of 18 km, 6 km, and 2 km, respectively. It carries a suite of TC-specific physics schemes with improved surface-exchange coefficients in the surface layer, and it also contains a vortex initialization scheme before the data assimilation that is first used to relocate the vortex in HWRF's preliminary background (which always comes from the GFS/GDAS or previous HWRF forecast cycle), and then to correct the size and intensity of the vortex with dynamic and thermodynamic consistency based on the National Hurricane Center (NHC) TC vital statistics (see details in Tallapragada et al., 2017). The boundary conditions for HWRF are provided by the GFS global forecasts. The NCEP ADP conventional data include land surface, marine surface, radiosonde, pibal and aircraft reports from the Global Telecommunications System (GTS), profiler and US radar derived winds, and satellite-derived winds that are assimilated routinely in operations (archived at http://rda.ucar.edu/datasets/ds337.0/). The CYGNSS data are available at CYGNSS official website (http://clasp-research.engin.umich.edu/missions/cygnss/).

The GSI-based 3DEnVar uses a variational framework with a hybrid of static and ensemble background error covariance terms. The configurations of the HWRF model and data assimilation system used in this study are similar to those of the NCEP 2017 operational HWRF system. One-way hybrid data assimilation is performed in the inner two nested domains of

HWRF (e.g., at 6 km and 2 km grid spacings, referred to as Ghost D02 and Ghost D03, respectively). For the hybrid background error covariance, a factor of 0.8 is used for ensemble covariance that comes from the 80-member Global Forecast System GFS EnKF data assimilation system.

Before assimilation, the CYGNSS OSWS data were thinned at 25 km resolution. The observation error was set to 2.1429 m s^{-1}, which was statistically defined in considering the errors of the maximum probability distribution of wind speed samples. More quality control steps (e.g., a gross check) were carried out inside GSI to exclude questionable observations, including some of the high wind speed (> 20 m s^{-1}) data. Less than 2% of thinned CYGNSS data were rejected during the data assimilation process.

2.3 Assimilation experiments

Three data assimilation experiments (DA_ADP, DA_CGS, DA_ALL) are conducted for comparison. DA_ADP acts as a control experiment and assimilates the NCEP ADP data that are routinely assimilated into the NCEP operational analysis, and Tail Doppler Radar (TDR) radial velocity when they are available from NOAA/HRD airborne mission. DA_CGS assimilates CYGNSS OSWS only. DA_ALL assimilates both CYGNSS OSWS and all data assimilated into DA_ADP. Note that for HWRF system, a vortex initialization (e.g., a vortex relocation and an intensity correction as mentioned above) is performed before the data assimilation in each analysis cycle when necessary (e.g., when storm center location and intensity differ from the TC vital data). Before the first cycled assimilation with CYGNSS data, the HWRF system is spin-up

for two days with 6-hourly analysis-forecast cycles that are similar to DA_ADP. Two sets of 6-hourly cycled data assimilation experiments are then performed. Each contains three assimilation experiments (DA_ADP, DA_CGS, DA_ALL) for comparison. The first set is for Hurricane Harvey, starting at 0600 UTC 21 August 2017, approximately five days ahead of landfall in Texas, and ending at 0600 UTC 24 August 2017. The second set is for the mature phase of Hurricane Irma before its Florida landfall. Similarly, the 6-hourly assimilation cycle starts at 0000 UTC 6 September 2017, which is also approximately five days ahead of landfall in southwestern Florida. A 126-hour forecast is made after data assimilation for each analysis cycle in all cases.

3. Results

3.1 Data impact on track and intensity forecasts

Figures 2a-c compare time evolution of the track and intensity between the best-track data and forecasts for Harvey initialized at 0600 UTC 21 Aug 2017 from all experiments. Generally, there is a positive impact of assimilation of CYGNSS OSWS (in both DA_CGS and DA_ALL) on track and intensity forecasts regarding both maximum surface wind (MSW) and minimum sea level pressure (MSLP). Compared with DA_ADP, the DA-CGS performs slightly better than DA_ALL, reflecting on complex combinations between vortex initialization and data assimilation during the analysis procedure. DA_ALL has a neutral impact of the track forecast of Irma (Figure 2d-f), while the DA_CGS slightly improved the track forecast. Meanwhile, assimilation of CYGNSS data had positive effects on the intensity forecast (DA_CGS and

DA_ALL), while DA_ALL perform better than DA_CGS in the intensity forecast for this case. All experiments capture the slowly weakening feature in the best-track analysis.

To obtain overall comparison among different experiments, and also to quantitatively evaluate the impact of OSWS on track and intensity forecasts, an improvement rate is introduced to measure improvements of the track and intensity in all the cycling analysis times over all forecast periods.

$$r_{track/intensity} = \left(err1_{track/intensity} - err2_{track/intensity}\right)/err1_{track/intensity} \times 100\%$$

where r represents the improvement rate, err1 is the track or intensity error in DA_ADP, and err2 is the track or intensity error in DA_CGS or DA_ALL. The subscript denotes that the improvement rate calculation for track and intensity uses the same equation; thus, a positive value means the track or intensity error in DA_ALL or DA_CGS less than that in DA_ADP.

Figure 3 shows the proportion of the number of experiments with a positive rate of improvement and averaged improvement rates at each forecast time. Out of the total 13 assimilation cycles, over 50% exhibit a positive impact on track forecasts at all forecast times. The average improvement rate fluctuates around 20% except for the 96-h to 126-h forecasts for Irma. As indicated by the colored numbers, the track improvements in the whole simulation period of Harvey and the first 66-hour forecasts of Irma are statistically significant according to a bootstrapping confidence test (Efron and Tibshirani, 1993). Note that forecast performance differs between Harvey and Irma after 90 hours. The improved proportion in both DA_CGS and DA_ALL dramatically decreases for Irma, which implies that CYGNSS

OSWS may be less capable of improving long-range track forecasts in the mature stage (e.g., Irma) of an intense hurricane, compared with one in the formation stage (e.g., Harvey). Although the proportion in DA_CGS often exceeds that in DA_ALL during the middle-range track forecast (18 to 54 hours) due to the complicated interactions between HWRF vortex initialization and data assimilation, MSW and MSLP forecasts in the 13 assimilation cycles (Figure 3b, c) indicate that DA_ALL shows an almost comparable average improvement rate to DA_CGS except for a few individual forecast hours. Meanwhile, the average proportion in DA_ALL is statistically significant when ignoring the MSW forecast of Irma, but not significant in DA_CGS, proving that less negative impacts on the intensity forecast in DA_ALL against these in DA_CGS and also implying that DA_ALL is still more reliable than DA_CGS overall. There is some inconsistency in the Irma MSW simulation, which may be because the best-track analysis dataset contains subjective uncertainties in estimating MSW.

3.2 Impact on hurricane inner-core structure

Figure 4 shows the wind in the low-level troposphere and the surface latent heat flux from HWRF simulations initialized at 0600 UTC 21 Aug for Harvey and at 0600 UTC 06 Sep 2017 for Irma, respectively. HWRF simulations are compared with airborne radar wind data from the NOAA Hurricane Research Division (HRD) at the closest time (Figure 4 a and b). Although the simulated wind speed is a bit stronger than that in the radar analysis, DA_ALL is the most consistent with the radar-observed patterns in wind structure. Specifically, in both the radar analysis and DA_ALL for Harvey, the maximum wind bands wrap around the northeast

side of the hurricane center. In the same comparison for Irma, DA_ALL also matches the radar analysis better in terms of location and size for the inner maximum wind band. The horizontal distribution of surface latent heat flux at the early time (6-h after analysis time; Figure 4 c and d) and also at the corresponding time (not shown) indicate that the maximum flux location and strength differ considerably between DA_ADP and DA_ALL. The asymmetric feature adjustments for the fluxes in DA_ALL and DA_CGS compared to DA_ADP should be of great help in reproducing the realistic wind structure.

Figure 5 compares the inner-core thermodynamic and kinematic aspects of Hurricanes Harvey and Irma at the same forecast time as in Figure 4a-b. The dropsonde data from reconnaissance aircraft missions collected by NOAA HRD are also used to verify simulations of the vertical structure (the last column of Figure 5). Distinct differences among the three assimilation experiments can be found. DA_ALL shows a more reasonable secondary circulation in the vortex core region and a distinct modification in the low-level inflow layer, and is more consistent with the dropsonde wind and temperature than DA_ADP, although there is a mixture impacts in some cases. At the same time, the middle to low-level warm core and moisture distribution change considerably between DA_ADP and DA_ALL. This suggests that assimilation of CYGNSS data with conventional data distinctly improves storm structure. In particular, the simulation accurately captures the asymmetrical distribution of the vortex circulation, which could be attributed to improvement in the hurricane vortex circulation and low-level heat and moisture adjustments around the inner-core region, as in Zhang et al. (2017).

Results above also consistent with previous studies (e.g., Kepert, 2017; Leslie and Smith, 1970) that hurricane intensity forecasts highly depend on low-level circulation and the surface dynamic conditions (e.g., OSWS) in the core region. Moreover, the DA_ALL are generally more reliable than DA_CGS, especially in the long-range forecast prove that the better representations of TC structure could improve hurricane forecasts (Chan, 2005).

4. Concluding remarks

2017 was the first Atlantic hurricane season in which the CYGNSS mission operated in its data-taking mode. This study demonstrated the potential positive impacts of CYGNSS data on the prediction of hurricane track and intensity by examining the assimilation of CYGNSS winds for two hurricane cases. Compared with the assimilation of conventional data, assimilation of CYGNSS winds is more effective in improving track forecasts, whereas the assimilation of both CYGNSS and conventional data has great potential to provide a better representation of vortex structure and is also helpful in producing a reasonable track forecast, especially in the medium range. Results also suggest that track forecasts could be affected by latent heat flux on the ocean surface and by TC structure, while intensity forecasts are highly dependent on the accuracy of the vortex structure. Future work should emphasize understanding the relevant details of the physical processes and merge the CYGNSS data with conventional data in the operational systems to obtain better track forecasts. More work should be done to comprehensively evaluate and compare data impacts using more cases and with the different version (e.g., Version 2.1) and type (e.g., YSLF) of the retrieved wind products and also with the different model systems to

better understand the processes associated with vortex and environmental flow that could be strongly influenced by CYGNSS data assimilation.

Acknowledgments.

This study is supported by the NASA NDOA program Award #NNX17AE95G and High-End Computing Program. The NASA CYGNSS science and operations teams are greatly appreciated for providing the data (https://podaac.jpl.nasa.gov/CYGNSS). The NCAR Developmental Testbed Center (https://dtcenter.org) is also acknowledged for supporting the HWRF and GSI software. NCEP ADP data are obtained from http://rda.ucar.edu/datasets/ds337.0/.

References

Annane, B., McNoldy, B., Leidner, S. M., Hoffman, R., Atlas, R., & Majumdar, S. J. (2018). A study of the HWRF analysis and forecast impact of realistically simulated CYGNSS observations assimilated as scalar wind speeds and as VAM wind vectors. *Monthly Weather Review*, 146, 2221-2236. https://doi.org/10.1175/MWR-D-17-0240.1

Atlas, R., Tallapragada, V., & Gopalakrishnan, S. (2015). Advances in tropical cyclone intensity forecasts. *Mar. Technol. Soc. J.*, 49, 149–160, http://doi:10.4031/MTSJ.49.6.2

Biswas, M. K., Carson, L., Newman, K., Bernardet, L., Kalina, E., & Grell, E. (2017). Community HWRF Users' Guide V3.9a, 160 pp. https://doi.org/10.7289/V5BC3WG5

Chan, J. C. L. (2005). The physics of tropical cyclone motion. *Annual Review of Fluid Mechanics*. 37, 99-128. https://doi.org/10.1146/annurev.fluid.37.061903.175702

Efron, B., and R. J. Tibshirani, 1993: *An Introduction to the Bootstrap*. Chapman and Hall, 436 pp.

Gall, R., Franklin, J., Marks, F., Rappaport, E. N., & Toepfer, F. (2013). The hurricane forecast improvement project. *Bulletin of the American Meteorological Society*, *94*(3), 329–343. https://doi.org/10.1175/BAMS-D-12-00071.1

Kepert, J. D. (2017). Time and space scales in the tropical cyclone boundary layer, and the location of the eyewall updraft. *Journal of the Atmospheric Sciences,*74, 3305-3323. https://doi.org/10.1175/JAS-D-17-0077.1

Leidner, S. M., Annane, B.,McNoldy, B., Hoffman, R., & Atlas, R. (2018). Variational analysis

of simulated ocean surface winds from the Cyclone Global Navigation Satellite System (CYGNSS) and evaluation using a regional OSSE. *Journal of Atmospheric and Oceanic Technology,* 35(8),1571-1584. http://doi:10.1175/JTECH-D-17-0136.1.

Leslie, L. M., & Smith, R. K. (1970). The surface boundary layer of a hurricane. II. *Tellus*, *20*(3), 288–297. https://doi.org/10.3402/tellusa.v22i3.10222

McNoldy, B., Annane, B., Majumdar, S. J., Delgado, J., Bucci, L., & Atlas, R. (2017). Impact of CYGNSS data on hurricane analyses and forecasts in a regional OSSE framework. *Marine Technology Society Journal*, 51(1), 7–15. https://doi.org/10.4031/MTSJ.51.1.1

Morris, M., & Ruf, C. S. (2017). Determining tropical cyclone surface wind speed structure and intensity with the CYGNSS satellite constellation. *Journal of Applied Meteorology and Climatology,* 56, 1847-1865. https://doi.org/10.1175/JAMC-D-16-0375.1

Otkin, J. A., Lewis, W. E., Lenzen, A. J., McNoldy, B. D., & Majumdar, S. J. (2017). Assessing the accuracy of the cloud and water vapor fields in the hurricane WRF (HWRF) model using satellite infrared brightness temperatures. *Monthly Weather Review,* 145, 2027-2046. https://doi.org/10.1175/MWR-D-16-0354.1

Pu, Z., Li, X., & Zipser, E. J. (2009) Diagnosis of the initial and forecast errors in the numerical simulation of rapid intensification of Hurricane Emily, *Weather and Forecasting*, 24, 1236-1251. https://doi.org/10.1175/2009WAF2222195.1

Pu, Z., Zhang, S., Tong, M., & Tallapragada, V. (2016). Influence of the self-consistent regional

ensemble background error covariance on hurricane inner-core data assimilation with the GSI-based hybrid system for HWRF. *Journal of the Atmospheric Sciences,* 73, 4911-4925. https://doi.org/10.1175/JAS-D-16-0017.1

Rogers, R.F., Aberson, S. D., Black, M. L., Black, P. G., Cione, J. J., Dodge, P. P., Dunion, J. P., Gamache, J. F., Kaplan, J., Powell, M. D., Shay, L. N., Surgi, N., & Uhlhorn, E. W. (2006). The Intensity Forecasting Experiment: A NOAA multi-year field program for improving tropical cyclone intensity forecasts. Bulletin of the American Meteorological Society, 87(11):1523-1537, doi:10.1175/BAMS-87-11-1523

Rogers, R., Aberson, S., Aksoy, A., Annane, B., Black, M., Cione, J., … Zhang, X. (2013). NOAA'S hurricane intensity forecasting experiment: A progress report. *Bulletin of the American Meteorological Society*, 94, 859–882. https://doi.org/10.1175/BAMS-D-12-00089.1

Ruf, C. S., Atlas, R., Chang, P. S., Clarizia, M. P., Garrison, J. L., Gleason, S., … Zavorotny, V. U. (2016). New ocean winds satellite mission to probe hurricanes and tropical convection. *Bulletin of the American Meteorological Society,* 3. 385-395. https://doi.org/10.1175/BAMS-D-14-00218.1

Ruf, C. S., & Balasubramaniam, R. (2018). Development of the CYGNSS geophysical model function for wind speed. *IEEE Journal of Selected Topics in Applied Earth Observations and Remote Sensing*. https://doi.org/10.1109/JSTARS.2018.2833075

Ruf, C. S., Gleason, S., & McKague, D. S. (2018). Assessment of CYGNSS wind speed retrieval

uncertainty. *IEEE Journal of Selected Topics in Applied Earth Observations and Remote Sensing*. https://doi.org/10.1109/JSTARS.2018.2825948

Tallapragada, V., Gopalakrishnan, S., Liu, Q., & Marchok, T. (2017). Hurricane Weather Research and Forecasting (HWRF) model: 2017 scientific documentation. *Developmental Testbed Center*, (August), 1–81. Retrieved from http://www.dtcenter.org/HurrWRF/users/docs/scientific_documents/HWRFScientificDocumentation_August2011.pdf

Wang, X., Parrish, D., Kleist, D., & Whitaker, J. (2013). GSI 3DVar-based ensemble–variational hybrid data assimilation for NCEP Global Forecast System: Single-resolution experiments. *Monthly Weather Review*. 41, 4098-4117. https://doi.org/10.1175/MWR-D-12-00141.1

Zhang, F., Weng, Y., Gamache, J. F., & Marks, F. D. (2011). Performance of convection-permitting hurricane initialization and prediction during 2008-2010 with ensemble data assimilation of inner-core airborne Doppler radar observations. *Geophysical Research Letters, 38*, L15810. https://doi.org/10.1029/2011GL048469

Zhang, S., Z. Pu, C. Velden, 2018: Impact of enhanced atmospheric motion vectors on HWRF hurricane analysis and forecasts with different data assimilation configurations. *Monthly Weather Review*, **146**, 1549-1569. https://doi.org/10.1175/MWR-D-17-0136.1

Zhang, S., Pu, Z., Posselt, D. J., & Atlas, R. (2017). Impact of CYGNSS ocean surface wind speeds on numerical simulations of a hurricane in observing system simulation experiments.

Journal of Atmospheric and Oceanic Technology, *34*(2), 375–383.

https://doi.org/10.1175/JTECH-D-16-0144.1

Figure Captions

Figure 1. (a) CYGNSS sample data swath at 00 UTC (blue), 06 UTC (green), 12 UTC (red), and 18 UTC (orange) on 06 September 2017. Bold, solid curves indicate tracks of Hurricanes Harvey and Irma during the time window of this study (track spans from 0600 UTC 21 to 1200 UTC 29 Aug 2017 for Harvey and from 0000 UTC 06 to 0000 UTC 12 Sep 2017 for Irma, respectively). The domain enclosed by the dashed line is the region for statistical calculations for (b) and (c). (b) Data count according to wind speed ranges during 0600 UTC 21 Aug to 0600 UTC 24 Aug 2017 (for Harvey; indicated by the blue line) and 0000 UTC 06 Sep to 0000 UTC 09 Sep 2017 (for Irma; denoted by the red line). The bar chart is similar to the lines but the total data count over the period of 0000 UTC 15 August to 0000 UTC 16 September 2017. The left vertical axis is the natural logarithm of the numbers for each wind speed range. (c) is similar to (b) except for scatterplots of CYGNSS wind speed versus standard deviation for Harvey (blue crosses), Irma (red crosses), and the total (black crosses).

Figure 2. Time series of the track(a) and intensity (b: MSW; c: MSLP) forecasts for Harvey (left column; initiated at 0600 UTC 21 Aug 2017) and Irma (right column; initiated at 0600UTC 06 Sep 2017). The colored number in each panel denotes the average absolute error for track and intensity over 126-h simulation for the experiments corresponding to the line colors.

Figure 3. Proportion of the number of experiments (bar chart; left Y-axis) in which the simulation errors in DA_CGS (blue) or DA_ALL (red) are less than those in DA_ADP at all forecast times for Harvey (left panel) and Irma (right panel) in terms of errors for track (top),

MSW (middle), and MSLP (bottom). Green solid and dashed lines with markers indicate the average improvement rate (right Y-axis) of DA_CGS and DA_ALL, respectively, for all analysis cycles in each forecast hour. The numbers in blue and red denote the average proportion of all positive track (a), MSW (b), and MSLP (c) impacts in DA_CGS and DA_ALL, over all forecast times for Harvey, and the first 66-hour forecasts for Irma, respectively. The single and double asterisks indicate that the average proportion is significant at the 75% and 90% confidence level, respectively, using the bootstrapping technique.

Figure 4. (a) and (b) are wind speeds (shaded contours) and vectors of (a) Harvey at 0600 UTC 25 Aug (96-h forecasts from 0600UTC 21 Aug 2017) and (b) Irma at 1200 UTC 08 Sep 2017 (54-h forecast from 0600UTC 06 Sep 2017) from experiments DA_ADP, DA_CGS, and DA_ALL, compared with HRD radar analysis at the 3 km and 4 km height level, respectively. (c) and (d) are corresponded 6-hour forecasts of surface latent heat flux initialed at the same time from experiments DA_ADP, DA_CGS, and DA_ALL for Harvey and Irma, respectively.

Figure 5. Comparison of the vertical cross section (left three columns) of azimuthally averaged hurricane vortices for Harvey (a-b) and Irma (c-d) from DA_ADP, DA_CGS, and DA_ALL at the same time as in Figure 4 (a and b). (a) and (c) depict the primary circulation denoted by tangential wind (m s^{-1}; colored shading) and secondary circulation represented by radial (m s^{-1}) and vertical 0.1 m s^{-1}) velocities. (b) and (d) are relative humidity (%, colored shading) and potential temperature anomaly (K, contours). The last column shows the vertical wind (a, c) and temperature (b, d) profiles of the dropsonde data from NOAA/HRD, compared with HWRF

simulations. Red, blue and black lines indicate the wind direction, wind speed, and temperature, respectively. For Harvey (and b), the dropsonde is located 39 km from the storm center at an azimuth angle of 317 degrees. For Irma (c and d), the dropsonde observation is located 154 km from the storm center at an azimuth angle of 126 degrees.

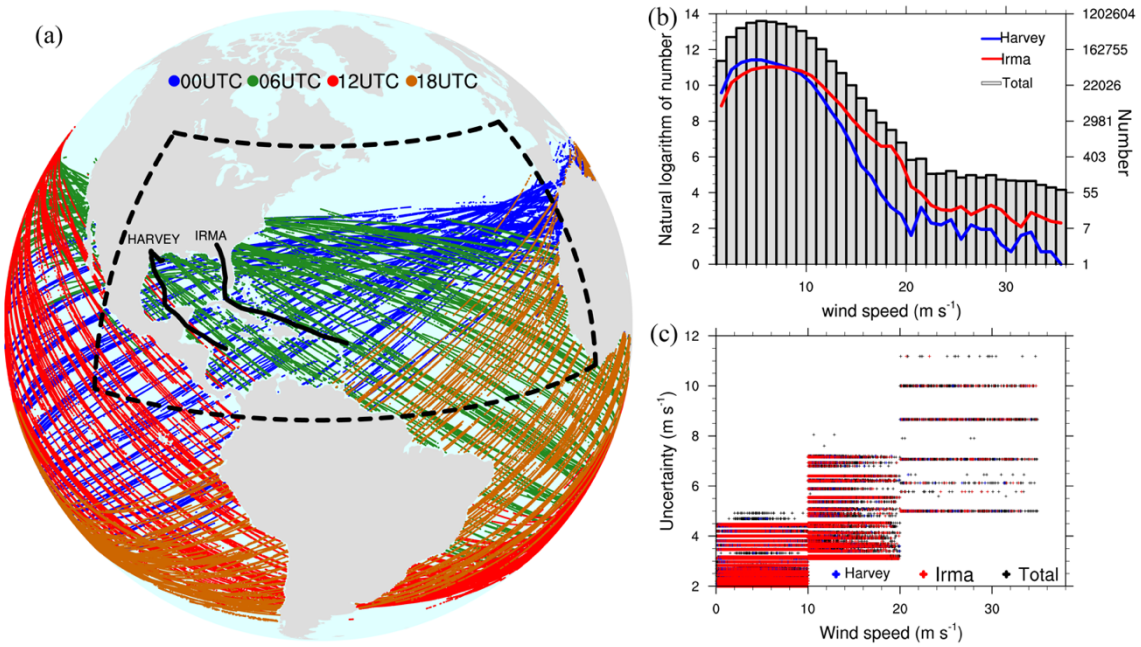

Figure 1. (a) CYGNSS sample data swath at 00 UTC (blue), 06 UTC (green), 12 UTC (red), and 18 UTC (orange) on 06 September 2017. Bold, solid curves indicate tracks of Hurricanes Harvey and Irma during the time window of this study (track spans from 0600 UTC 21 to 1200 UTC 29 Aug 2017 for Harvey and from 0000 UTC 06 to 0000 UTC 12 Sep 2017 for Irma, respectively). The domain enclosed by the dashed line is the region for statistical calculations for (b) and (c). (b) Data count according to wind speed ranges during 0600 UTC 21 Aug to 0600 UTC 24 Aug 2017 (for Harvey; indicated by the blue line) and 0000 UTC 06 Sep to 0000 UTC 09 Sep 2017 (for Irma; denoted by the red line). The bar chart is similar to the lines but the total data count over the period of 0000 UTC 15 August to 0000 UTC 16 September 2017. The left vertical axis is the natural logarithm of the numbers for each wind speed range. (c) is similar to

(b) except for scatterplots of CYGNSS wind speed versus standard deviation for Harvey (blue crosses), Irma (red crosses), and the total (black crosses).

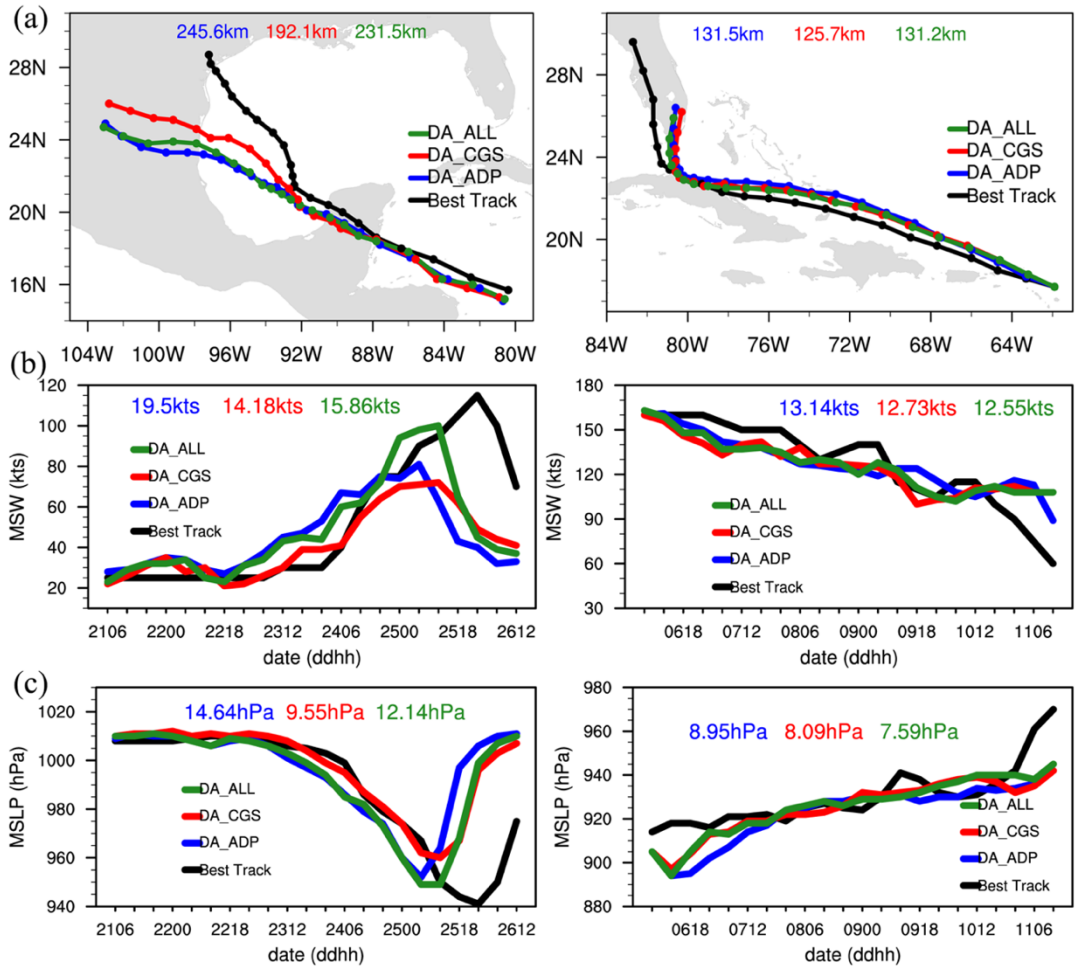

Figure 2. Time series of the track(a) and intensity (b: MSW; c: MSLP) forecasts for Harvey (left column; initiated at 0600 UTC 21 Aug 2017) and Irma (right column; initiated at 0600UTC 06 Sep 2017). The colored number in each panel denotes the average absolute error for track and

intensity over 126-h simulation for the experiments corresponding to the line colors.

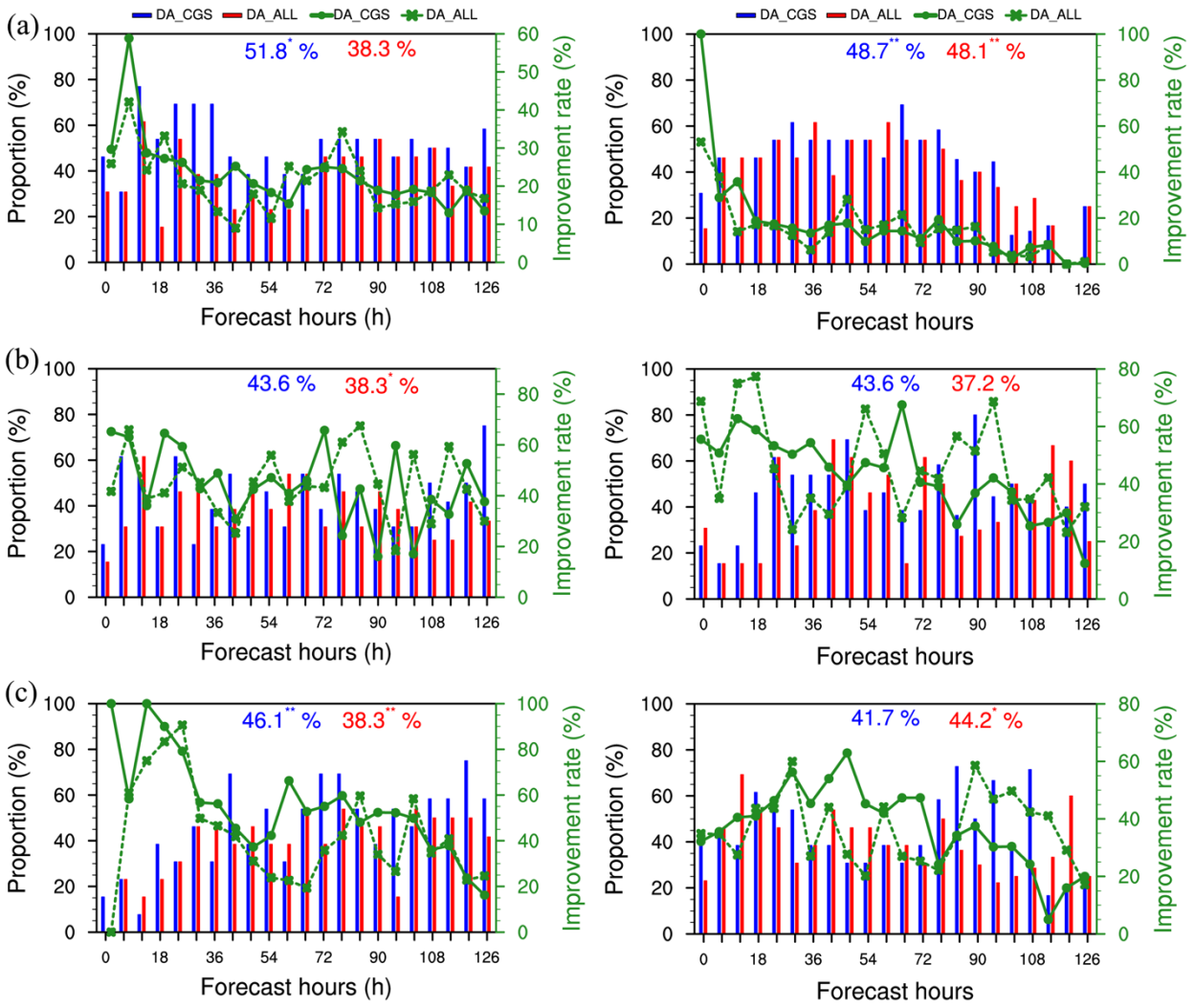

Figure 3. Proportion of the number of experiments (bar chart; left Y-axis) in which the simulation errors in DA_CGS (blue) or DA_ALL (red) are less than those in DA_ADP at all forecast times for Harvey (left panel) and Irma (right panel) in terms of errors for track (top), MSW (middle), and MSLP (bottom). Green solid and dashed lines with markers indicate the average improvement rate (right Y-axis) of DA_CGS and DA_ALL, respectively, for all analysis cycles in each forecast hour. The numbers in blue and red denote the average proportion of all

positive track (a), MSW (b), and MSLP (c) impacts in DA_CGS and DA_ALL, over all forecast times for Harvey, and the first 66-hour forecasts for Irma, respectively. The single and double asterisks indicate that the average proportion is significant at the 75% and 90% confidence level, respectively, using the bootstrapping technique.

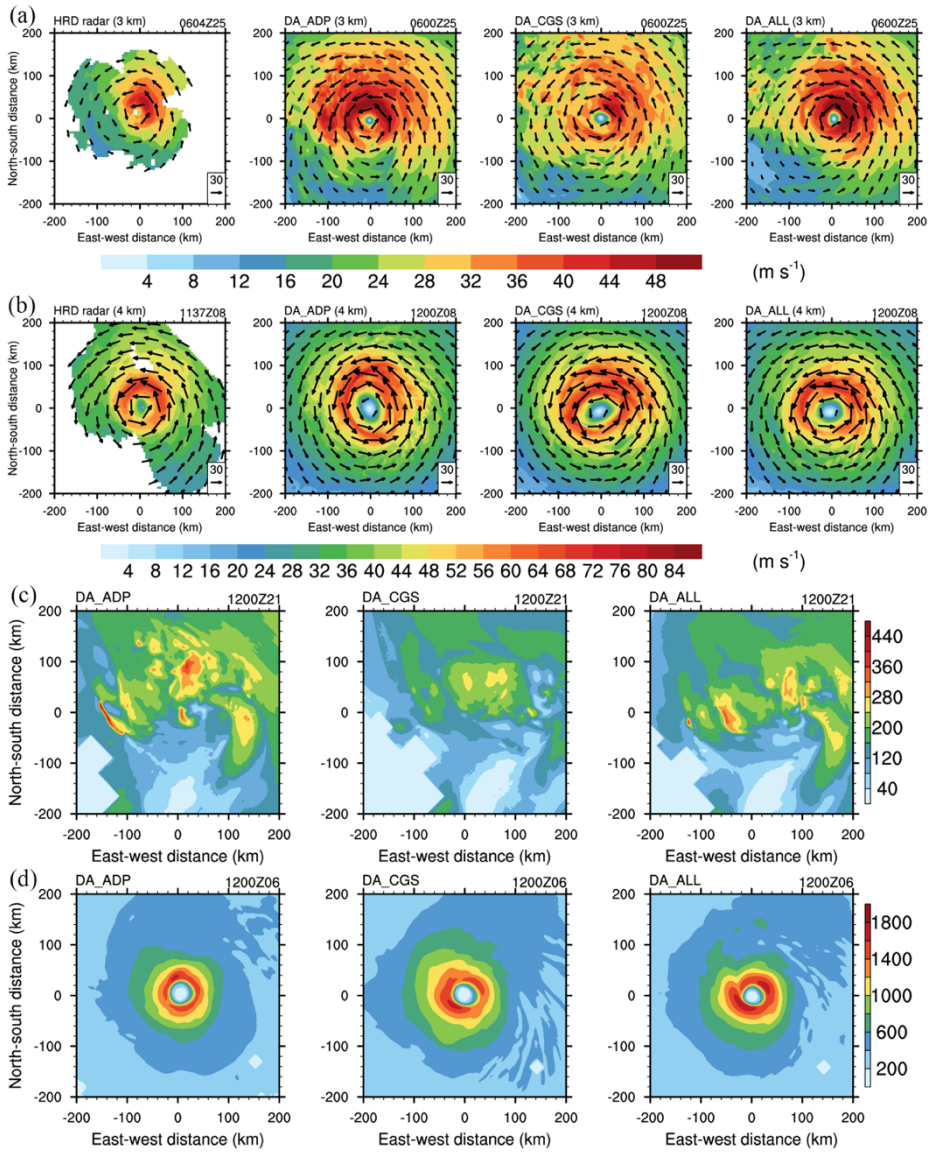

Figure 4. (a) and (b) are wind speeds (shaded contours) and vectors of (a) Harvey at 0600 UTC 25 Aug (96-h forecasts from 0600UTC 21 Aug 2017) and (b) Irma at 1200 UTC 08 Sep 2017 (54-h forecast from 0600UTC 06 Sep 2017) from experiments DA_ADP, DA_CGS, and DA_ALL, compared with HRD radar analysis at the 3 km and 4 km height level, respectively.

(c) and (d) are corresponded 6-hour forecasts of surface latent heat flux initialed at the same time from experiments DA_ADP, DA_CGS, and DA_ALL for Harvey and Irma, respectively.

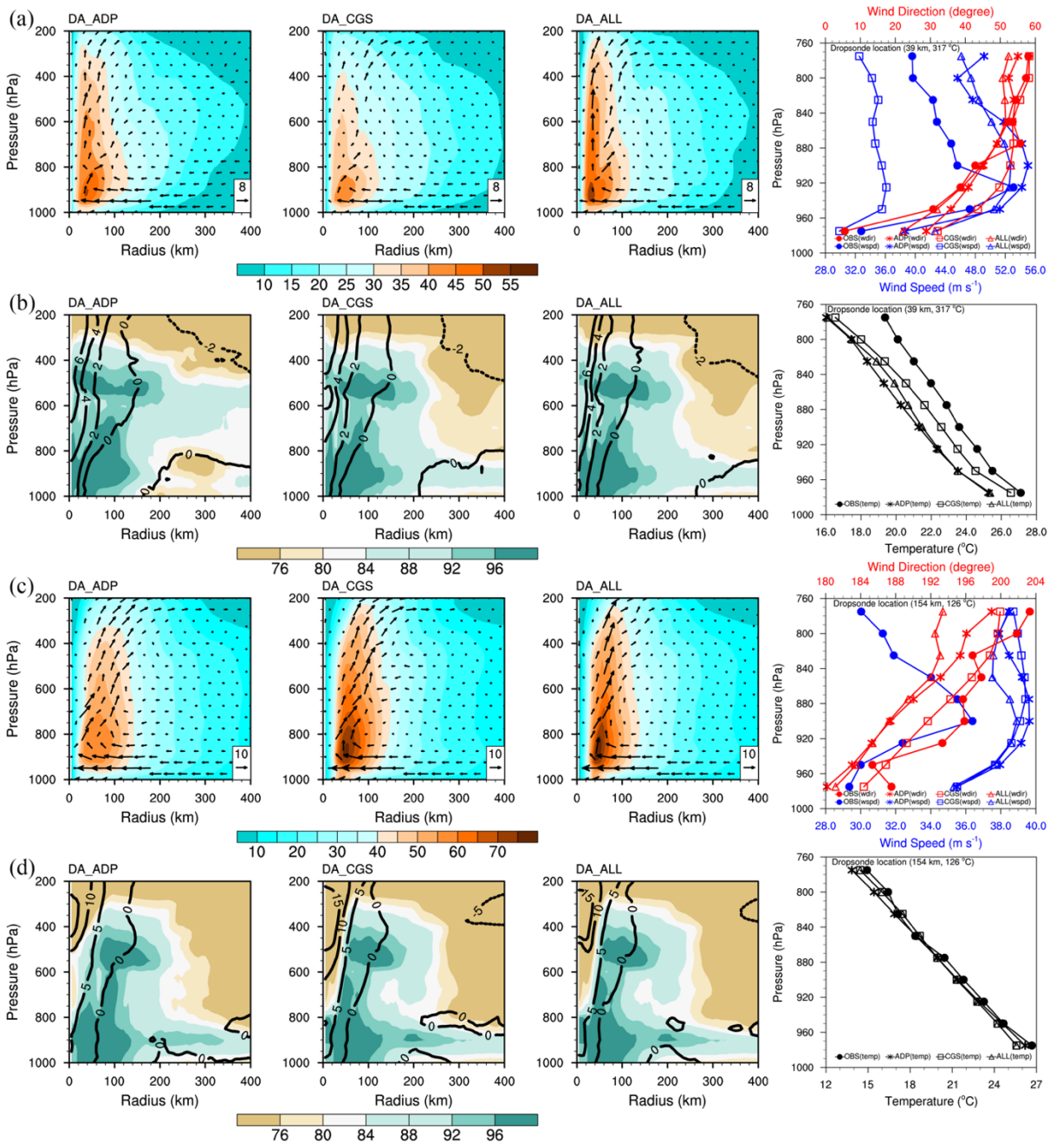

Figure 5. Comparison of the vertical cross section (left three columns) of azimuthally averaged hurricane vortices for Harvey (a-b) and Irma (c-d) from DA_ADP, DA_CGS, and DA_ALL at

the same time as in Figure 4 (a and b). (a) and (c) depict the primary circulation denoted by tangential wind (m s^{-1}; colored shading) and secondary circulation represented by radial (m s^{-1}) and vertical (0.1 m s^{-1}) velocities. (b) and (d) are relative humidity (%, colored shading) and potential temperature anomaly (K, contours). The last column shows the vertical wind (a, c) and temperature (b, d) profiles of the dropsonde data from NOAA/HRD, compared with HWRF simulations. Red, blue and black lines indicate the wind direction, wind speed, and temperature, respectively. For Harvey (and b), the dropsonde is located 39 km from the storm center at an azimuth angle of 317 degrees. For Irma (c and d), the dropsonde observation is located 154 km from the storm center at an azimuth angle of 126 degrees.

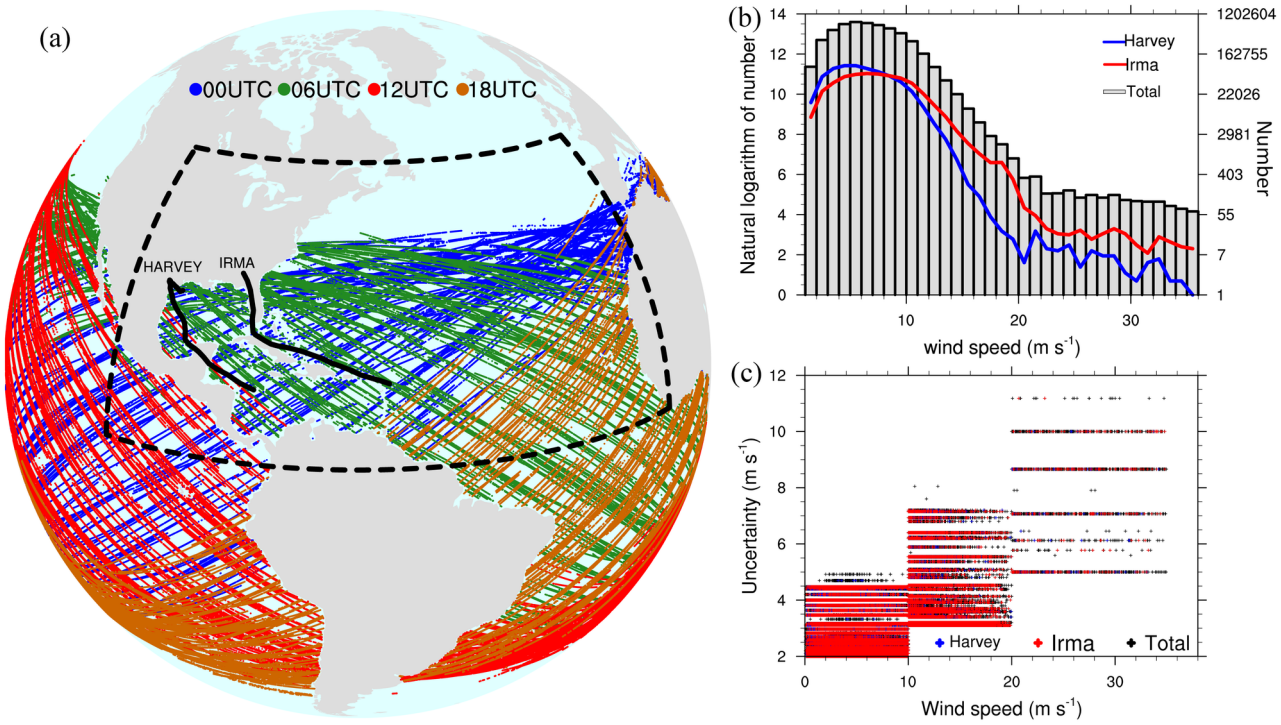

2019GL082236-f01-z-.tif

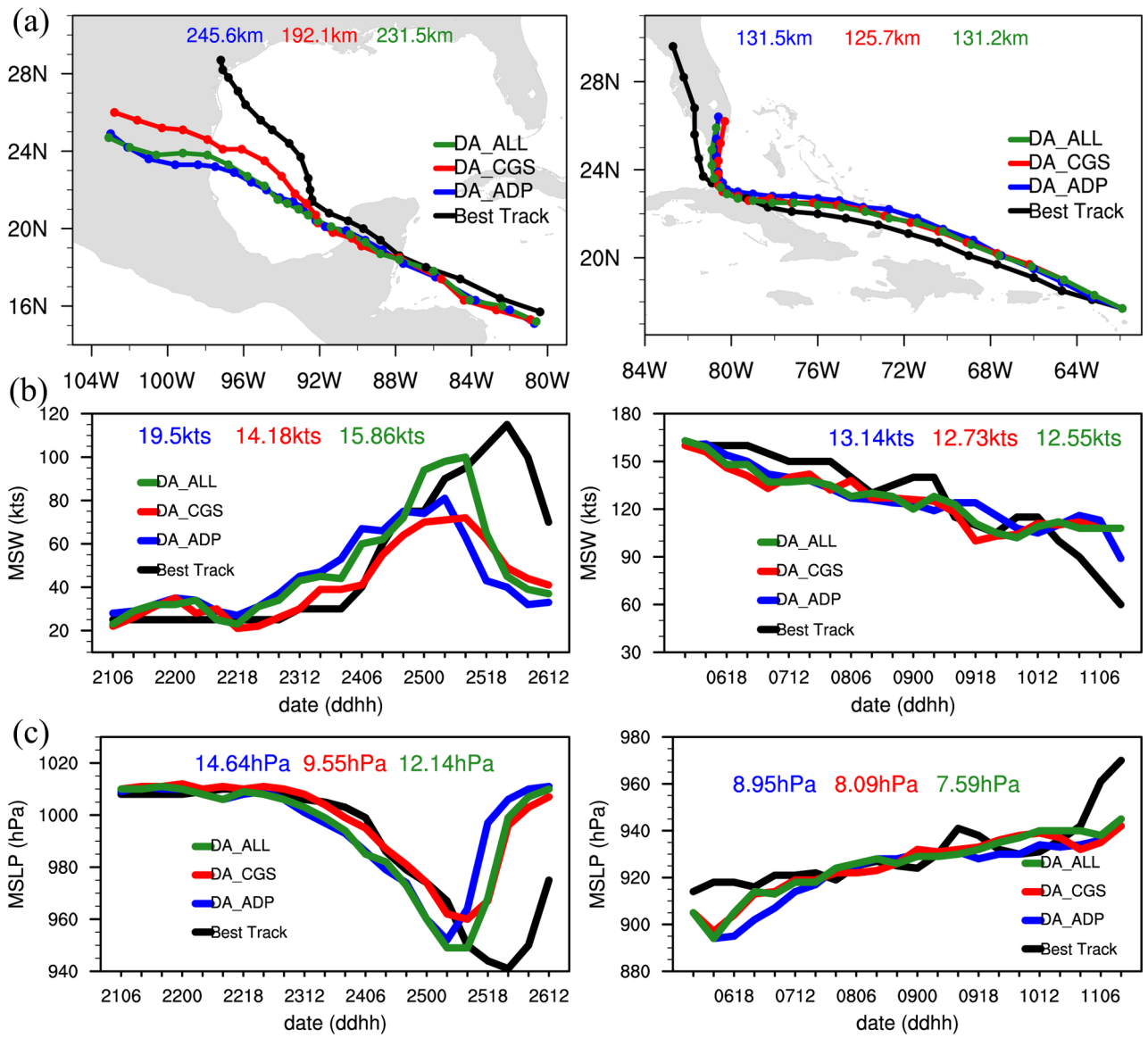

2019GL082236-f02-z-.tif

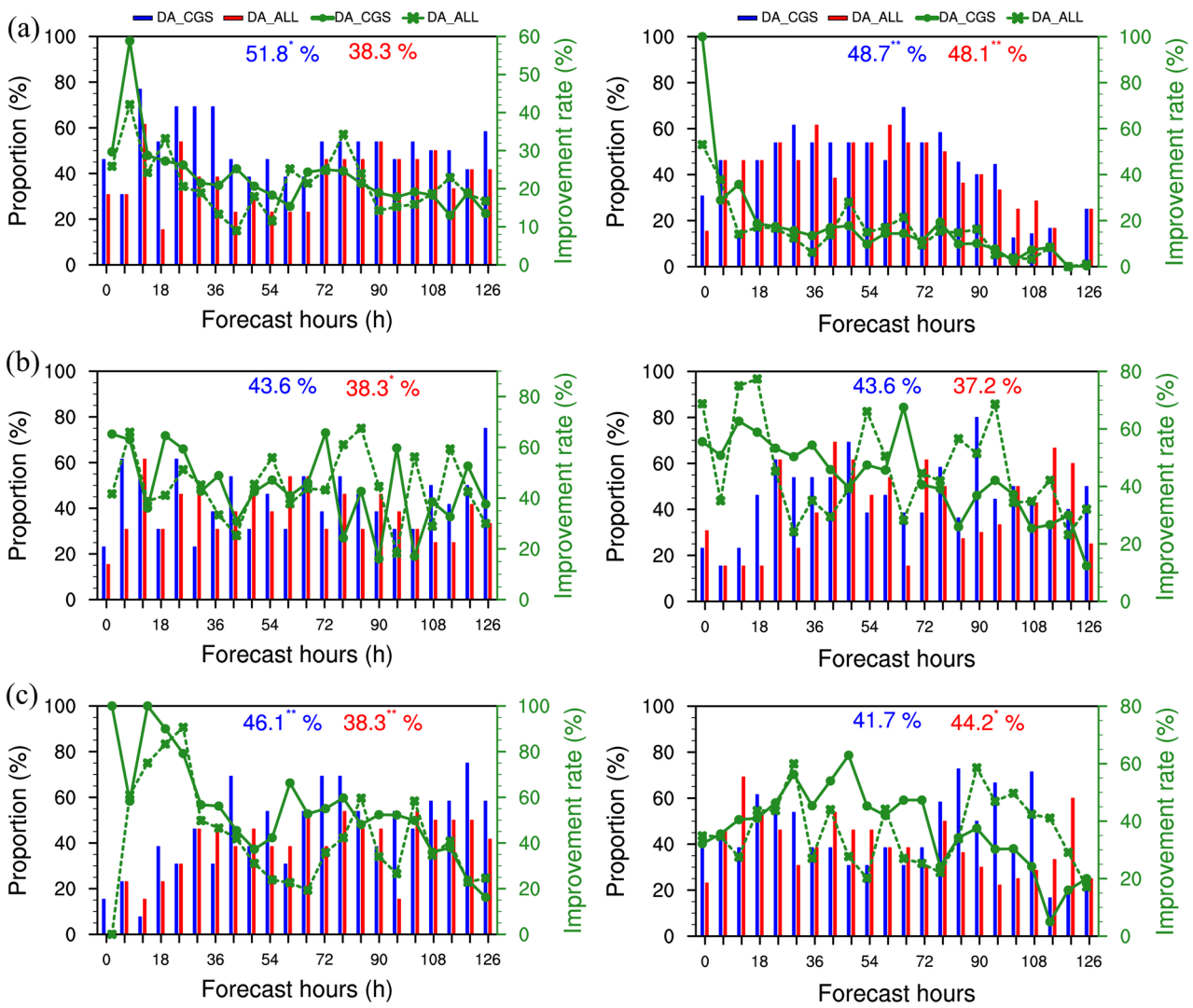

2019GL082236-f03-z-.tif

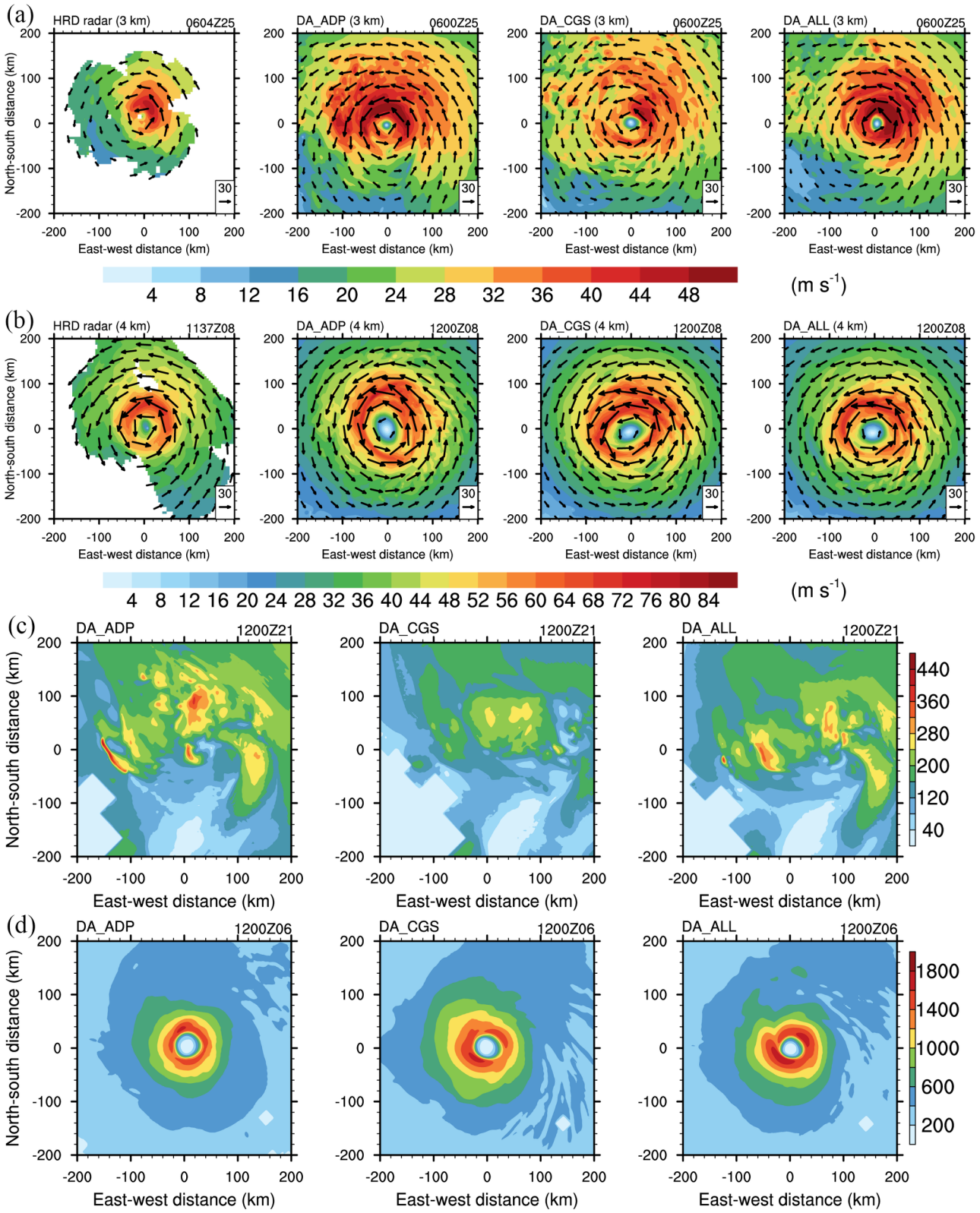

2019GL082236-f04-z-.tif

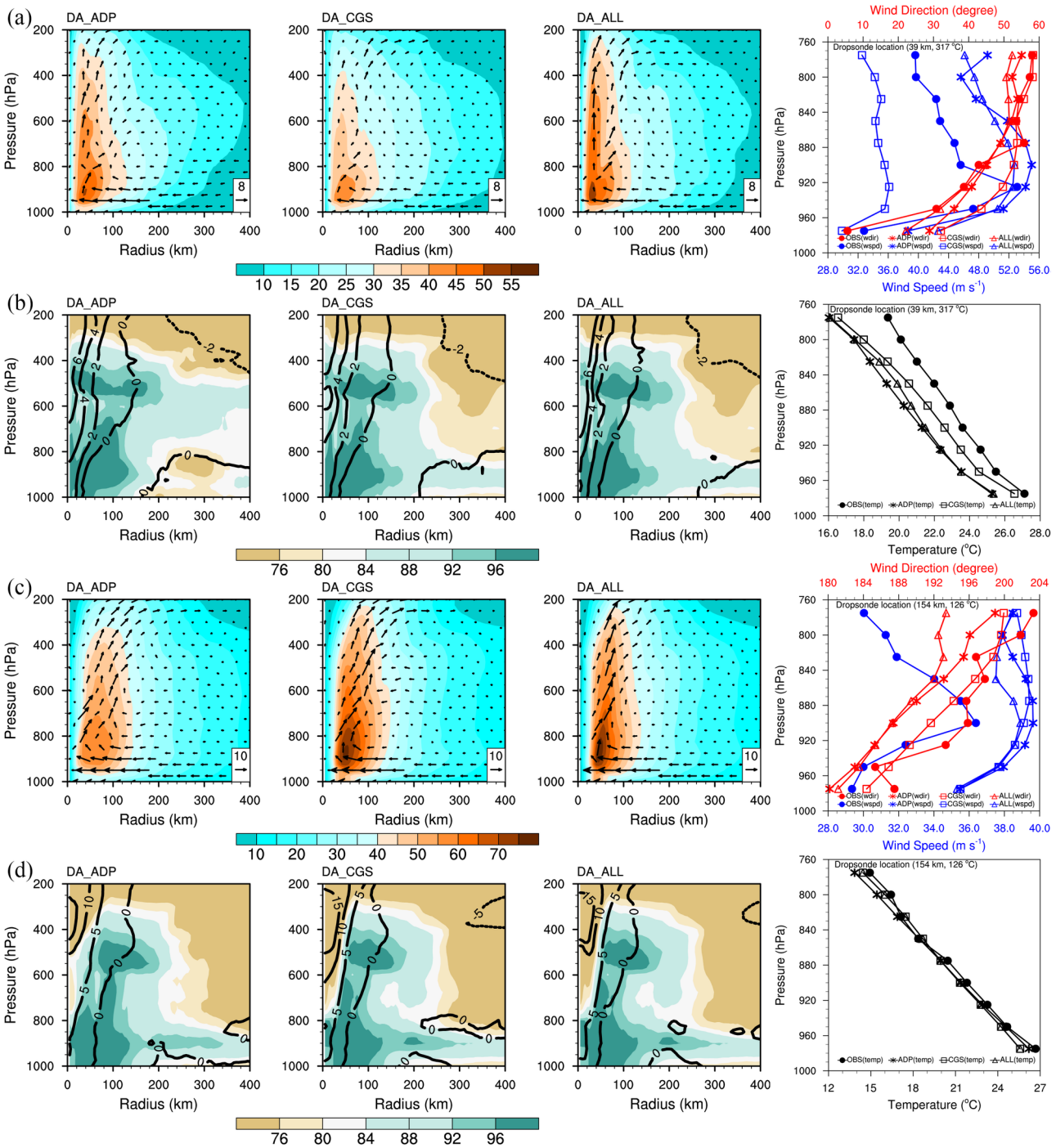

2019GL082236-f05-z-.tif